The JCMT Nearby Galaxies Legacy Survey – XI. Environmental variations in the atomic and molecular gas radial profiles of nearby spiral galaxies

Angus Mok,[1]★ C. D. Wilson,[1] J. H. Knapen,[2,3] J. R. Sánchez-Gallego,[4] E. Brinks[5] and E. Rosolowsky[6]

[1]*Department of Physics and Astronomy, McMaster University, Hamilton, ON L8S 4M1, Canada*
[2]*Instituto de Astrofísica de Canarias, E-38205 La Laguna, Tenerife, Spain*
[3]*Departamento de Astrofísica, Universidad de La Laguna, E-38200 La Laguna, Tenerife, Spain*
[4]*Department of Physics and Astronomy, University of Kentucky, 40506-0055, Lexington, Kentucky, USA*
[5]*Centre for Astrophysics Research, University of Hertfordshire, AL10 9AB Hatfield, Hertfordshire, UK*
[6]*Department of Physics, University of Alberta, Edmonton, AB T6G 2R3, Canada*

ABSTRACT

We present an analysis of the radial profiles of a sample of 43 H I-flux selected spiral galaxies from the Nearby Galaxies Legacy Survey (NGLS) with resolved James Clerk Maxwell Telescope (JCMT) CO $J = 3 - 2$ and/or Very Large Array (VLA) H I maps. Comparing the Virgo and non-Virgo populations, we confirm that the H I discs are truncated in the Virgo sample, even for these relatively H I-rich galaxies. On the other hand, the H_2 distribution is enhanced for the Virgo galaxies near their centres, resulting in higher H_2 to H I ratios and steeper H_2 and total gas radial profiles. This is likely due to the effects of moderate ram pressure stripping in the cluster environment, which would preferentially remove low-density gas in the outskirts while enhancing higher density gas near the centre. Combined with Hα star formation rate data, we find that the star formation efficiency (SFR/H_2) is relatively constant with radius for both samples, but the Virgo galaxies have an ∼40 per cent lower star formation efficiency than the non-Virgo galaxies.

Key words: stars: formation – ISM: molecules – galaxies: ISM – galaxies: spiral.

1 INTRODUCTION

In the Universe, galaxies can be found in many different environments, from isolated galaxies, to groups of tens of galaxies, to clusters of thousands of galaxies. The star formation histories of these galaxies have been observed to vary greatly due to their environment. For example, overdense regions are increasingly dominated by quiescent galaxies (Dressler 1980; Blanton & Moustakas 2009). One of the major questions in the study of galaxy evolution is whether these effects are due to processes intrinsic to the galaxy, such as through the process of 'mass quenching', or if they can be attributed to the local environment (Peng et al. 2010, 2012). The lower density group environment is also important in this analysis, as galaxies can begin to be quenched in these groups before falling into clusters (McGee et al. 2009).

Optical studies of galaxies at a range of redshifts have provided valuable insight into these environmental effects, but a full analysis requires the study of the fuel for ongoing and future star formation.

Spiral galaxies are important to this analysis because they are sites of active star formation, with gaseous discs that are sensitive to the effects of their surroundings. Past studies of the H I content of spiral galaxies in clusters have found that they are deficient in atomic gas (Haynes & Giovanelli 1986) and their gas distributions are significantly truncated (Cayatte et al. 1990).

More recent studies have shown that star formation is most closely linked to the molecular gas content in these galaxies (Leroy et al. 2008; Bigiel et al. 2011; Saintonge et al. 2011). Given the observed reduction in overall star formation inside cluster spirals (Koopmann, Haynes & Catinella 2006), the cluster environment should therefore have a strong effect on their molecular gas content. Processes such as ram pressure stripping (Gunn & Gott 1972), tidal harassment (Moore et al. 1996) and strangulation (Larson, Tinsley & Caldwell 1980) have been proposed to explain the environment's influence on the more diffuse H I component. However, any potential environmental effects on the denser, more centrally located H_2 gas is less clear.

Initial observations by Kenney & Young (1989) for 40 Virgo spirals using the Five College Radio Astronomy Observatory (FCRAO) found that they are not as H_2 deficient as they are H I deficient and

★ E-mail: mokakf@mcmaster.ca

suggested the survival of a large amount of molecular gas inside these galaxies. More recently, the Herschel Virgo Cluster Survey (HeViCS) created a sample of 12 galaxies with CO measurements and found that for disturbed galaxies, the H I gas is more efficiently stripped than the H_2 gas (Pappalardo et al. 2012). This results in steeper H_2 and total gas radial profiles for the more H I-deficient galaxies in their sample. The Herschel Reference Survey (HRS), which is a *K*-band selected sample of nearby galaxies, used the H I-deficiency parameter as a proxy for galaxy interactions and found a correlation between H I deficiency and the level of H_2 gas deficiency and H_2 gas disc size (Boselli et al. 2014). They suggested that the Virgo spiral galaxies may be more H_2 deficient than unperturbed field galaxies.

Here, we take a slightly different approach by using a gas-rich sample of spiral galaxies in three different environments (field, group and the Virgo Cluster), which should be better proxies for any immediate environmental effects. To study the molecular gas properties of these galaxies, we use resolved maps from the Nearby Galaxies Legacy Survey (NGLS), an H I-flux limited sample of 155 nearby ($D < 25$ Mpc) galaxies (Wilson et al. 2012). In a previous paper, we select spiral galaxies from the NGLS sample to compare the field, group and Virgo subsamples, focusing on their integrated properties (Mok et al. 2016). Compared to the non-Virgo galaxies, galaxies in the Virgo Cluster have higher H_2 gas masses and H_2 to H I ratios, perhaps due to environmental interactions that aid in the conversion of atomic to molecular gas. They also have lower specific star formation rates (sSFR = SFR$/M_*$) and lower star formation efficiencies (SFR$/M_{H_2}$), implying molecular gas depletion times ($t_{gas} = M_{H_2}/$SFR) that are longer than those of the non-Virgo galaxies.

In this paper, we further investigate the environmental effects by studying the radial profiles of the NGLS galaxies and measure any differences between the Virgo and non-Virgo sample. We select 43 galaxies from the larger sample of NGLS spiral galaxies for which we have detected maps of their H_2 and/or H I distributions, while excluding galaxies with inclinations of greater than 75°. In Section 2, we present our observations and some of the general properties of our sample. In Section 3, we discuss the procedure used to create the radial profiles. We also present radial profiles for the H_2, H I and star formation rate surface densities, as well as combinations of these properties, such as the molecular gas depletion time. Then, we discuss some implications of our data and provide comparisons to other observational and theoretical results.

2 OBSERVATIONS AND ANALYSIS

2.1 Data and sample selection

We seek to create a large sample of spiral galaxies with resolved molecular and/or atomic gas data available. To the original NGLS sample (Wilson et al. 2012), we add galaxies that match the NGLS survey criterion from two follow-up James Clerk Maxwell Telescope (JCMT) programmes. The first is a programme to complete the H I-flux selected sample of galaxies in the Virgo Cluster (M09AC05) and the second is to map the galaxies from the HRS (M14AC05). From this larger sample, we select only spiral galaxies using the HyperLeda data base, excluding any elliptical or lenticular galaxies. This results in the 98 spiral galaxies used in the analysis from Mok et al. (2016). For all of the galaxies in the survey, the CO $J = 3 - 2$ line was mapped out to at least $D_{25}/2$ using HARP on the JCMT (Wilson et al. 2012). The D_{25} value for each galaxy, which we take from the HyperLeda survey, is defined as the length

of the major axis of a galaxy at the *B*-band isophotal level of 25 mag arcsec^{-2} (Paturel et al. 2003). In our analysis, we also use R_{25}, which is half of the D_{25} value for each galaxy.

To study the resolved properties of these galaxies, we select only galaxies for which we have detections in the CO $J = 3 - 2$ maps from the JCMT and/or the H I 21 cm line from the Very Large Array (VLA). We exclude all galaxies with inclinations of greater than 75°, as measured by the HyperLeda data base (Paturel et al. 2003; Makarov et al. 2014), to remove any galaxies that are close to an edge-on configuration and not appropriate for our radial profile analysis. Our final resolved sample contains 43 galaxies.

In total, there are 33 galaxies with CO $J = 3 - 2$ detections from the JCMT. One of the main advantages to our molecular gas data set is that the observations were all made using the same instrument, in the same CO transition, and with the same survey specifications. This homogeneous data set provides a good basis for comparison between the different galaxies and different environments. The CO $J = 3 - 2$ data reduction process is described in Wilson et al. (2012) and will not be repeated here. A full analysis of the integrated properties of the spiral galaxies in this sample can be found in Mok et al. (2016).

For the H I data, we have collected maps from the VLA for 25 galaxies. First, we use data from the VLA Imaging of Virgo in Atomic Gas (VIVA) survey (Chung et al. 2009), where we have downloaded the moment zero maps from their website[1] for the 14 galaxies that overlap with the NGLS sample. Most of these observations were taken with the VLA in the B- or C-array configuration, with some beam sizes approaching the 15 arcsec resolution of the JCMT. There is also one galaxy, NGC3077, with H I data from the THINGS survey[2] (Walter et al. 2008). We observed an additional 10 NGLS galaxies with the VLA in the D-array configuration (VLA Project Identifier: AW701, 15B-111). The six AW701 galaxies were reduced manually using CASA while the newer four 15B-111 galaxies were reduced using the automated VLA pipeline. To create the integrated H I intensity maps, we also perform a -1σ to 1σ noise cut on the data cube. We present images of the integrated intensity (moment zero) maps for these 10 galaxies in Fig. 1.

For the star formation rate data, we use the Hα observations from Sánchez-Gallego et al. (2012), which presented the star formation properties of the galaxies in the NGLS using a combination of archival data and new observations. We use the reduced FITS files, corrected using the *R*-band continuum filter and the provided conversion factor between Hα counts and Hα flux to convert the original image into units of the star formation rate. The full procedure to correct the Hα maps for contamination from the [N II] lines and the process to estimate the A(Hα) factor, the internal absorption of Hα, can be found in Sánchez-Gallego et al. (2012).

We supplement this with Hα data from the HRS (Boselli et al. 2015), where we download the Hα images from their website.[3] We also include observations for one galaxy (NGC4273) from the Hα3 survey, taken from the GOLDMINE data base (Gavazzi et al. 2012). For these galaxies, we first measure the Hα counts for the galaxies using an aperture created by eye to capture most of the flux from these galaxies. We combine this information with the published Hα flux values to determine the appropriate conversion factor. In order to maintain continuity with the previous papers in this series, we follow the procedure outlined in

---

[1] http://www.astro.yale.edu/viva/

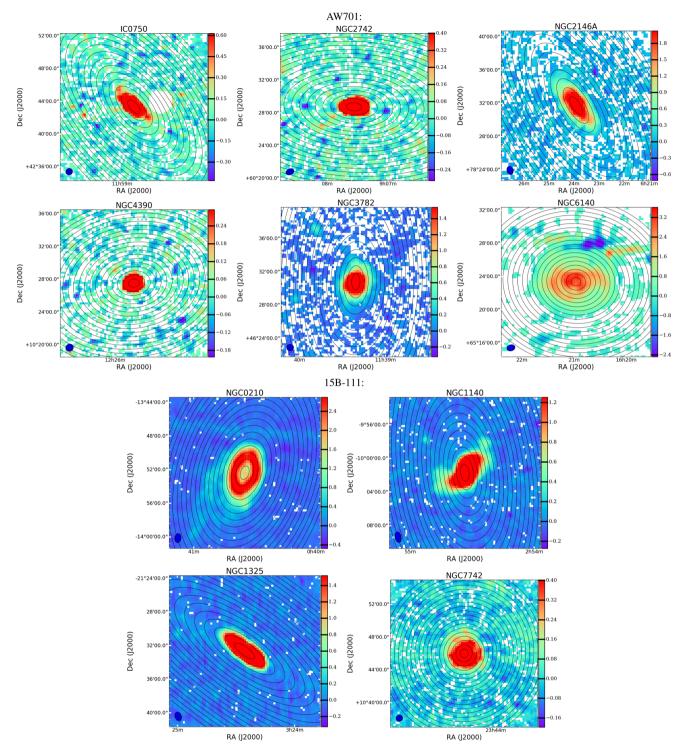[2] http://www.mpia.de/THINGS/Overview.html

[3] http://hedam.lam.fr/HRS/

Figure 1. The H I 21 cm moment zero maps of the galaxies from the AW701 and 15B-111 VLA programmes, in units of Jy beam^{-1} km s^{-1}. The annuli used for the creation of the radial profiles are overlaid in black and the beam is shown in the lower left corner of each image. The six AW701 galaxies are presented first, followed by the 15B-111 galaxies.

Sánchez-Gallego et al. (2012) to correct the Hα flux for [N II] contamination and A(Hα) factor. For many of these galaxies, we also had to manually align the Hα maps, as coordinate information was not included in the FITS files. For those cases, we compared to Digital Sky Survey images of the galaxies and fit to star positions using at least five stars for each image.

In summary, there are 25 galaxies with H I maps, 33 with H$_2$ maps and 43 with Hα maps. More information about the sample can be found in Table 1, where the individual galaxies are listed, along with their available data sets, their inclinations and physical distances. Full tables of the key physical properties of the spiral galaxies in our sample can be found in Mok et al. (2016).

Table 1. Available H I, H₂ and Hα data for the galaxies in our sample.

Galaxy[1]	Env[2]	H I source	H I beam size[3]	H I rms[3] [mJy beam^{-1}]	H₂[4]	Hα	Incl [°]	Dist [Mpc]
NGC0210	F	15B-111	66 arcsec × 46 arcsec	1.75	D	HRS	55.4	22.4
NGC3437	F	–	–	–	D	HRS	72.8	20.1
NGC6140	F	AW701	60 arcsec × 45 arcsec	2.16	ND	NGLS	32.2	17.8
NGC7742	F	15B-111	51 arcsec × 49 arcsec	1.57	D	HRS	16.8	24.8
IC0750	G	AW701	51 arcsec × 49 arcsec	1.30	D	NGLS	65.8	8.3
IC3908	G	–	–	–	D	HRS	73.2	19.0
NGC0450	G	–	–	–	D	NGLS	49.8	25.4
NGC1140	G	15B-111	79 arcsec × 44 arcsec	1.51	ND	NGLS	73.8	20.1
NGC1325	G	15B-111	66 arcsec × 47 arcsec	1.74	ND	NGLS	74.3	20.7
NGC2146A	G	AW701	63 arcsec × 46 arcsec	1.50	ND	NGLS	69	25.9
NGC2742	G	AW701	62 arcsec × 45 arcsec	1.24	D	NGLS	60.6	22.4
NGC3077	G	THINGS	14 arcsec × 13 arcsec	0.94	D	NGLS	38.1	3.9
NGC3162	G	–	–	–	D	NGLS	37.1	20.7
NGC3227	G	–	–	–	D	NGLS	68.3	18.4
NGC3346	G	–	–	–	D	HRS	34.1	19.5
NGC3507	G	–	–	–	D	NGLS	31.9	15.5
NGC3684	G	–	–	–	D	HRS	50.8	18.4
NGC3782	G	AW701	51 arcsec × 49 arcsec	1.26	ND	NGLS	60.3	14.3
NGC3982	G	–	–	–	D	HRS	29.9	20.1
NGC4041	G	–	–	–	D	NGLS	22	21.9
NGC4123	G	–	–	–	D	HRS	44.3	20.1
NGC4713	G	VIVA	26 arcsec × 22 arcsec	1.96	D	HRS	23.8	10.9
NGC4771	G	–	–	–	D	HRS	74.4	17.2
NGC4772	G	VIVA	18 arcsec × 15 arcsec	0.36	ND	NGLS	67.3	16.1
NGC4775	G	–	–	–	D	HRS	28.4	23.0
NGC4808	G	VIVA	40 arcsec × 36 arcsec	0.59	D	HRS	69.2	12.0
NGC4254	V	VIVA	38 arcsec × 33 arcsec	0.41	D	NGLS	20.1	16.7
NGC4273	V	–	–	–	D	GOLDMINE	26.9	16.7
NGC4294	V	VIVA	29 arcsec × 27 arcsec	0.29	ND	HRS	70.2	16.7
NGC4298	V	VIVA	17 arcsec × 16 arcsec	0.35	D	NGLS	58.4	16.7
NGC4303	V	–	–	–	D	HRS	18.1	16.7
NGC4383	V	VIVA	45 arcsec × 38 arcsec	0.26	D	NGLS	63.7	16.7
NGC4390	V	AW701	58 arcsec × 53 arcsec	1.16	ND	NGLS	43.3	16.7
NGC4396	V	VIVA	27 arcsec × 27 arcsec	0.28	ND	HRS	71.6	16.7
NGC4430	V	–	–	–	D	NGLS	43.8	16.7
NGC4480	V	–	–	–	D	HRS	61.2	16.7
NGC4548	V	VIVA	17 arcsec × 16 arcsec	0.30	ND	HRS	36.9	16.7
NGC4567	V	VIVA	17 arcsec × 16 arcsec	0.36	D	NGLS	39.4	16.7
NGC4568	V	VIVA	17 arcsec × 16 arcsec	0.36	D	NGLS	67.5	16.7
NGC4579	V	VIVA	42 arcsec × 35 arcsec	0.45	D	NGLS	41.9	16.7
NGC4647	V	–	–	–	D	NGLS	31.6	16.7
NGC4651	V	VIVA	17 arcsec × 16 arcsec	0.40	D	NGLS	49.5	16.7
NGC4654	V	VIVA	16 arcsec × 16 arcsec	0.45	D	HRS	59.8	16.7

Notes. [1]Galaxies with both H I and H₂ data are in bold face.

[2]For the environment, F indicates field galaxies, G indicates group galaxies and V indicates the Virgo galaxies.
A full explanation of our categories can be found in Mok et al. (2016).

[3]Beam sizes and rms from the H I maps in the VIVA survey are from table 2 of Chung et al. (2009).

[4]For H₂ data, D indicates detected galaxies, ND indicates non-detected galaxies.

2.2 Integrated properties of the resolved sample

2.2.1 Comparison with the remaining NGLS spiral galaxies

First, we compare our resolved subset of 43 galaxies to the remaining sample of 55 NGLS spiral galaxies from Mok et al. (2016) that were not included in this paper, as they did not possess detected CO $J = 3 - 2$ emission or VLA H I observations or they have high inclinations. We find that the two samples have similar H I gas masses (log $M_{H_I} = 9.16 \pm 0.05$ for the resolved sample versus log $M_{H_I} = 9.05 \pm 0.04$ for the non-included sample). The similar total H I gas mass is likely due to the H I flux selection imposed by the NGLS. We also find no significant difference between the integrated H I properties of the Virgo galaxies in the resolved sample, compared to the Virgo galaxies that were not included in this paper. These results indicate that we are not selecting a potentially biased H I sample out of the original H I-flux selected sample.

On the other hand, the stellar masses for the resolved sample (log $M_* = 9.94 \pm 0.06$) are significantly higher than those for the non-included sample (log $M_* = 9.37 \pm 0.07$). In Mok et al. (2016), we found that the stellar mass for the CO $J = 3 - 2$ detected galaxies is significantly higher than the stellar mass for the CO $J = 3 - 2$

Table 2. Global properties of the non-Virgo and Virgo resolved samples.

Mean quantity	Non-Virgo (26)	Virgo (17)	KS test
$\log M_{\mathrm{H\,I}}$ [$M_\odot$]	9.24 ± 0.05	9.04 ± 0.08	<u>0.009</u>
$\log M_*$ [$M_\odot$]	9.87 ± 0.07	10.05 ± 0.12	0.154
$M_{\mathrm{H\,I}}/M_*$	0.35 ± 0.06	0.15 ± 0.03	0.108
Distance [kpc]	18.6 ± 0.94	16.0	–
$\log$ SFR [$M_\odot$ yr^{-1}]	-0.29 ± 0.09	-0.25 ± 0.14	0.774
$\log$ sSFR [yr^{-1}]	-10.17 ± 0.09	-10.30 ± 0.10	0.610
$\log M_{\mathrm{H\,I}}/$SFR [yr]	9.54 ± 0.07	9.29 ± 0.11	0.486
$\log M_{\mathrm{H_2}}{}^1$ [$M_\odot$]	8.35 ± 0.11	8.83 ± 0.13	<u>0.028</u>[2]
$\log$ SFR$/M_{\mathrm{H_2}}{}^1$ [yr]	-8.62 ± 0.11	-9.06 ± 0.10	<u>0.049</u>[2]
$M_{\mathrm{H_2}}/M_*{}^1$	0.047 ± 0.012	0.095 ± 0.016	0.051[2]
$M_{\mathrm{H_2}}/M_{\mathrm{H\,I}}{}^1$	0.38 ± 0.14	1.43 ± 0.37	<u>0.007</u>[2]
$M_{\mathrm{H_2}} + M_{\mathrm{H\,I}}$ [$M_\odot$]^1	9.35 ± 0.05	9.35 ± 0.10	0.656[2]

Notes. Underline indicates $p < 0.05$.
[1] CO non-detections taken into account using survival analysis;
please refer to Mok et al. (2016) for more information.
[2] Log-rank test used, which takes into account censored data.

non-detected galaxies. Thus, it is not surprising to see a similar difference in stellar mass, since this resolved sample would comprise most of the CO $J = 3 - 2$ detected galaxies, except for a few heavily inclined galaxies. In addition, the star formation rates are higher in the resolved sample. This is likely due to the strong link between H$_2$ gas and star formation, as well as between stellar mass and star formation. These results suggest that the resolved sample would not contain many of the gas-rich low surface brightness galaxies discussed in Mok et al. (2016) and in other surveys of these H I-rich objects, such as HIghMass (Huang & Kauffmann 2014).

2.2.2 Comparison of the Virgo and non-Virgo galaxies in the resolved sample

For our resolved sample, we present a summary of the global properties of the non-Virgo and Virgo galaxies in Table 2. In this analysis, we have combined the field and group galaxy samples to increase the number of galaxies in the non-Virgo sample.

Although the non-Virgo galaxies have higher H I masses, the difference in the stellar mass normalized H I masses is less significant, as shown by performing the Kolmogorov–Smirnov test on the two distributions. While Virgo galaxies have a higher average stellar mass, it is less than a 1σ difference and the Kolmogorov–Smirnov test shows that the two distributions cannot be distinguished. The other properties, such as star formation rate and specific star formation rate (sSFR), are also comparable between the two samples. These results give us more confidence that we are comparing between similar galaxies and probing the more subtle effects of environment.

The main difference between the Virgo and non-Virgo resolved samples is in the molecular gas properties. Since not all of these galaxies are detected in the CO $J = 3 - 2$ maps, as shown in Table 1, we have used the statistical technique of survival analysis on these two samples, as discussed in Mok et al. (2016). The resolved sample shows the same general trends as analysis from the full NGLS sample, with the Virgo galaxies possessing higher mean molecular gas masses, higher H$_2$ to H I ratios and lower star formation efficiencies (or longer molecular gas depletion times). For the total gas mass, the two samples are quite similar, suggesting that the cluster environment may be aiding in the conversion process between atomic

and molecular gas. We will further explore these global results by measuring the radial profiles of these galaxies.

2.3 Creating surface density maps

We convert the HARP CO $J = 3 - 2$ moment maps to an H$_2$ surface density map by assuming a CO to H$_2$ conversion factor of $X_{\mathrm{CO}} = 2 \times 10^{20}$ cm^{-2}(K km s^{-1})$^{-1}$ (Strong et al. 1988) or $\alpha_{\mathrm{CO}} = 3.2\ M_\odot$ pc^{-2}(K km s^{-1})$^{-1}$. We use a constant line ratio (R_{31}) between CO $J = 3 - 2$ and CO $J = 1 - 0$ of 0.18, the average value found for galaxies in the NGLS (Wilson et al. 2012). This leads to the following relation between $\Sigma_{\mathrm{H_2}}$, the surface density of molecular hydrogen, and $I_{\mathrm{CO(3-2)}}$, the integrated CO $J = 3 - 2$ intensity:

$$\Sigma_{\mathrm{H_2}}[M_\odot\ \mathrm{pc}^{-2}] = 17.8 \times (R_{31}/0.18)^{-1} I_{\mathrm{CO(3-2)}}[\mathrm{K\ km\ s^{-1}}] \quad (1)$$

To convert the VLA 21 cm moment zero maps into physical units, we combine equations 1 and 5 from Walter et al. (2008) and then convert to units of $M_\odot$ pc^{-2}. This leads to the following relationship, where Σ_{HI} is the surface density of H I, $\sum S\Delta \nu$ is the integrated flux density from the moment zero maps and FWHM$_{\mathrm{maj}} \times$ FWHM$_{\mathrm{min}}$ is a measure of the beam area:

$$\Sigma_{\mathrm{HI}}[M_\odot\ \mathrm{pc}^{-2}] = 8765.27 \times \frac{\sum S\Delta \nu [\mathrm{Jy\ beam^{-1}\ km\ s^{-1}}]}{\mathrm{FWHM}_{\mathrm{maj}} \times \mathrm{FWHM}_{\mathrm{min}}}, \quad (2)$$

For the Hα maps, we convert the Hα counts into star formation rates using the procedure outlined in Section 2.1. This process uses the conversion factor from Kennicutt et al. (2009), which assumes a Kroupa IMF (Kroupa & Weidner 2003):

$$\mathrm{SFR}[M_\odot\ \mathrm{yr}^{-1}] = 5.5 \times 10^{-42}\ \mathrm{L(H}\alpha)[\mathrm{erg\ s^{-1}}] \quad (3)$$

where SFR is the star formation rate and L(Hα) is the Hα luminosity. When we generate radial profiles, we divide the star formation rates in each measured annulus by its physical size, as determined by the distance to each galaxy listed in Table 1. This results in a final measurement of the surface density of star formation (Σ_{SFR}) in units of $M_\odot$ yr^{-1} pc^{-2}.

We perform an additional data reduction step on the CO $J = 3 - 2$ and Hα data. Our VLA data set has a wide variety of angular resolutions while our CO $J = 3 - 2$ data set has a constant angular resolution of 15 arcsec. To allow for analysis using a combination of two values (such as the H$_2$/H I ratio) and to better compare between the H$_2$ and H I data sets, we adopted a standard 60 arcsec resolution. For the galaxies observed using the D-array configuration, we convolved the CO $J = 3 - 2$ and Hα maps to the same resolution as the H I maps using the software package STARLINK. For the VIVA data set, observed using the VLA in the B/C configurations, we convolved all three maps (H$_2$, H I and Hα) to our standard 60 arcsec resolution.
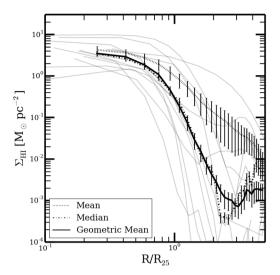
Finally, we correct for any inclination effects by multiplying our resulting maps with a $\cos i$ factor, with the inclinations provided from the HyperLeda data base (Paturel et al. 2003).

2.4 Generating radial profiles

To generate the radial profiles for our galaxies, we use the coordinates, position angle and inclination data from the HyperLeda data base to define 20 concentric annuli. The widths of each ring along the minor axis is set to 30 arcsec, which is half of the standard angular resolution for our data set. We then measure the mean values within each aperture using the APPERADD command. For galaxy pairs that were collected in a single map, such as NGC4567 and
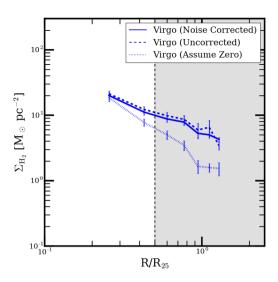
Figure 2. Left: a comparison of the results from using different methods for defining the radial profile for the population of the Virgo galaxies, including mean (dotted), geometric mean (solid) and median (dot–dashed). Error bars for the mean are statistical. Error bars for the median method are based on median absolute deviation. Error bars for the geometric mean method are based on the formula from Norris (1940). We see that the mean profile is biased by high outliers, while the median method produces jagged profiles in regions due to a small number of galaxies. Right: the average H_2 surface density radial profiles, measured using the geometric mean method, for the Virgo galaxies in our sample. The radii are normalized by R_{25}. The dashed vertical line is at $R_{25} = 0.5$, the main target area of the NGLS survey, and results from the CO $J = 3 - 2$ maps are less reliable in the shaded region. The original, uncorrected profile (dashed line), the noise-corrected profile (solid line) and the profile assuming blank pixels have no gas (dotted line) are plotted. The three methods produce similar results in the reliable region near the centre, where most of the CO $J = 3 - 2$ pixels are detected.

NGC4568, the other galaxy was masked out manually from the individual maps. We note that the radial profiles will only extend as far out as the observed area in each map and may not include all 20 annuli, especially for the H_2 data.

Furthermore, an annulus is only included if it contains more than 5 per cent valid (non-blank) pixels. We have tested more conservative thresholds, such as 25 per cent, and it did not result in any significant difference in our profiles and results. However, it did reduce the amount of galaxies in our H_2 sample due to the localized nature of some of our CO $J = 3 - 2$ detections. To maximize the number of galaxies in our sample, we have maintained this low threshold.

To determine any systematic difference between the galaxies in the sample, we divide the physical radii by each galaxy's R_{25}, which is half of their D_{25} value from the HyperLeda data base. This normalization is important because the Virgo galaxies in our sample are on average slightly closer and physically larger than the galaxies in the non-Virgo sample (Mok et al. 2016). A comparison using physical radii (kpc) may be affected by the differences in the size of the galaxies in the Virgo and non-Virgo samples and their distances.

Next, we tested three ways of combining the profiles to create the 'average' radial profile for our subsamples: the median, the mean and the geometric mean. The geometric mean is the square root of the product of the input values. This is also equivalent to the log-average, where we perform the arithmetic mean on the logarithmic values.

We calculate the average profile at equally spaced points in the R_{25}-normalized radius, interpolating between the physical annuli points where necessary. The results of these three methods for the H I data are presented in the left plot of Fig. 2 for the Virgo sample. These averages are only calculated in regions where there are more than three galaxies. The differences in the horizontal range that each radial profile spans depend on the number of

galaxies in each sample and the interaction between the fixed size annuli used for the analysis and the distance to each individual galaxy.

The error bars on the mean are the statistical errors and the error bars on the median are based on the median absolute deviation. The error on the geometric mean uses the formula from Norris (1940):

$$S_G = G \frac{s_{\log x_i}}{\sqrt{n-1}}, \tag{4}$$

where G is the geometric mean, $s_{\log x_i}$ is the standard deviation of the log values and n is the number of galaxies. Since the stellar masses of the Virgo and non-Virgo samples are not significantly different and we are normalizing their radii using R_{25}, we can compare the standard error on the mean values of these similar objects. Note that the data points where we calculate the average profile will correspond to different points at the R/R_{25} for each individual galaxy, given their varying distances and sizes. Thus, we perform interpolation between the measured annuli points for the individual galaxy profiles when necessary. It is also possible for the error bars to be underestimated, because each data point in an average profile is not fully independent of the others. On the other hand, this is compensated by the large number of individual galaxy profiles that goes into the averaging process.

We chose the geometric mean method to generate the average radial profile for our analysis. Compared to the median method, it provides a more stable profile. The median can produce ragged profiles, particularly at radii with few individual measurements. Compared to the mean method, the geometric mean is more representative. The simple mean can be biased by high outliers, especially when presented in a log–log plot. The choice of the particular averaging method does not change the overall results presented in this paper, especially between the median and the geometric mean methods.
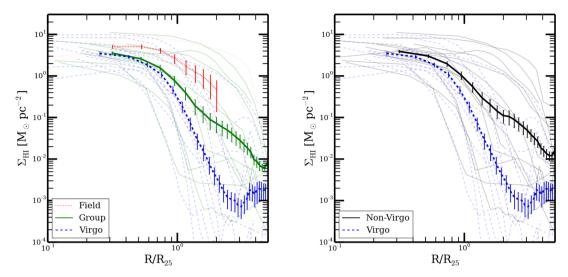
Figure 3. The radial profiles of H I surface density for the galaxies in our sample, calculated using the geometric mean method and normalized by R_{25}. The statistical error bars for each profile are plotted. The individual galaxy profiles are in the background. Left: the sample is separated into field (red-dotted), group (green) and Virgo (blue-dashed) populations. We see a reduction in the sizes of the H I disc, from field to group to the Virgo Cluster, suggesting H I properties are affected even in moderate density environments. Right: the sample is separated into the non-Virgo (black) and Virgo (blue-dashed) populations. Even for this H I-flux selected sample, the Virgo Cluster galaxies have truncated H I distributions in the outskirts compared to the non-Virgo galaxies.

Finally, we calculate the average R/R_{25} value for the galaxies in each average radial profile. To create a balance between the increased data set available from combining our individual profiles and the angular resolution of our data, we decided to generate average radial profile points at intervals that are the equivalent of 15 arcsec at the average R/R_{25} value for the galaxies making up the average profile.

2.5 Correcting blank pixels in H$_2$ maps

The CO $J = 3 - 2$ maps for many of our galaxies contain large areas of blank pixels. This is due to the sensitivity limits of the observations and the data reduction procedure from Wilson et al. (2012), which removes regions of the map below a certain signal-to-noise limit. One approach is to assume that the non-detected pixels have no molecular gas present. This correction is performed by multiplying the raw value by the ratio of valid pixels to the total number pixels in the aperture. This can be considered a lower limit to the H$_2$ profile. Another approach is to add in the average 1σ noise of the map for those missing pixels. This second correction method assumes that the undetected pixels would take on the mean value from the noise map generated in the data reduction process, where a line width of 100 km s^{-1} is assumed. The final approach is to make no corrections to the average value of the detected pixels measured in the aperture, which we will call the uncorrected profile.

We compare these three methods to correct for these blank pixels in the right plot of Fig. 2, looking at the H$_2$ radial profiles for our Virgo sample. These corrections are not very important within $R/R_{25} = 0.5$, the main target area of the NGLS survey. Inside this region, most of the pixels are detected and the three curves are similar to each other. We decided to apply the noise correction method to all of the subsequent H$_2$ maps in our sample, as this is the most physical scenario. In general, the noise-corrected profile provides similar results to the uncorrected case. The radial profile for the case where we assume no molecular gas is present in the

blank pixels naturally produces steeper profiles, as it reduces the surface density in the outskirts of these galaxies.

3 RESULTS AND DISCUSSION

3.1 H I radial profiles – stripping in the group and Virgo galaxies

We present the radial profiles for our sample of galaxies with available H I data in Fig. 3. We separate the sample of galaxies by field, group and Virgo samples and also between the Virgo and non-Virgo samples. All of the radial profiles have a relatively flat inner portion, which transitions into a steeper profile in the outskirts. We note that the galaxies in the Virgo Cluster have truncated H I discs compared to non-Virgo galaxies, which was seen in previous studies of Virgo Cluster spirals (Cayatte et al. 1994). The new result here is that this truncation is seen even in this sample of H I-flux selected galaxies from the NGLS.

Comparing the smaller field and group samples, the field galaxies have a shallower decrease in the outskirts compared to the group galaxies. This would suggest a natural trend in H I disc sizes from the field to the group and then to the cluster environment. Given we only have three field galaxies with H I maps in our sample, we may need more observations to confirm this difference with the group sample. On the other hand, this scenario fits well with the picture of ram pressure stripping, where higher density environments can strip away the interstellar medium (ISM) of spiral galaxies. Our result provides some more evidence for H I stripping in environments of relatively modest density. Observationally, H I-deficient galaxies have been found in the group environment, such as in Hickson Compact Groups (Martinez-Badenes et al. 2012). The Blind Ultra Deep H I Environmental Survey (BUDHIES) has also found a correlation between the fraction of H I-detected galaxies and the mass of their host groups (Jaffé et al. 2016).

In addition, since this is an H I-flux selected sample from the NGLS, these galaxies still possess a relatively large amount of
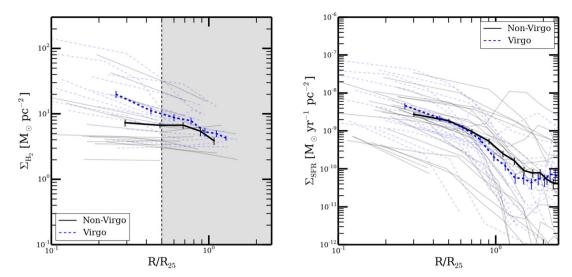
Figure 4. Left: the radial profiles of H_2 surface density for the galaxies in our sample, calculated using the geometric mean method and normalized by R_{25}. The statistical error bars for each profile are plotted. The individual galaxy profiles are in the background. The sample is separated into the non-Virgo (black) and Virgo (blue-dashed) populations. The dashed vertical line is at $R_{25} = 0.5$, the main target area of the NGLS survey, and results from the CO $J = 3 - 2$ maps are less reliable in the shaded region. On average, the Virgo galaxies are more H_2-rich at all radii, along with a steeper radial gradient. Right: the radial profiles of star formation rate surface density for the galaxies in our sample, calculated using the geometric mean method and normalized by R_{25}. The statistical error bars for each profile are plotted. The individual galaxy profiles are in the background. We see an enhancement in the star formation rates near the centre of Virgo galaxies, similar to the behaviour of the H_2 distribution. However, there are also hints of a truncation in their discs at large radii.

available cold gas. It is likely that the NGLS is preferentially selecting galaxies that are recently infalling into the Virgo Cluster or have not been strongly affected by the cluster environment. In addition, due to the H I-flux criteria and with most of the galaxies in the resolved sample detected in the CO $J = 3 - 2$ maps, we are selecting relatively high stellar mass galaxies that are less likely to be fully stripped according to semi-analytical models (Luo et al. 2016). Despite these caveats, the trends observed in the H I radial profile suggest that the environment can still play a big factor in changing the spatial distribution of the ISM inside these galaxies.

3.2 H_2 radial profiles – enhancement in the Virgo galaxies

The H_2 radial profiles are presented in the left plot of Fig. 4. With the small number of CO-detected field galaxies and the short range over which we have enough galaxies to generate an average radial profile, the remaining figures will only show a comparison between the Virgo sample and the combined field and group samples. Comparing between the Virgo and non-Virgo samples, we see that the H_2 disc is not significantly truncated for the Virgo galaxies. In fact, the H_2 surface density is enhanced near the centre. This is consistent with results from the integrated measurements (Mok et al. 2016), where we noted an increase in the H_2 gas mass for the Virgo galaxies in this H I-flux selected sample.

As discussed in Section 3.1, the NGLS is an H I-flux selected survey and likely contains galaxies not yet strongly affected by the cluster environment. As a result, our sample may not be directly comparable to those from the HeViCS or the HRS, which contain a large population of H I-deficient objects that are also often H_2 deficient. Our results suggest that for recently infalling galaxies or galaxies in less extreme environments, molecular gas can be enhanced rather than reduced by the cluster environment.

A comparison of the H_2 and H I profiles for Virgo galaxies suggests that while the environment can play a role in truncating the H I discs in these galaxies, some of the gas may lose angular mo-
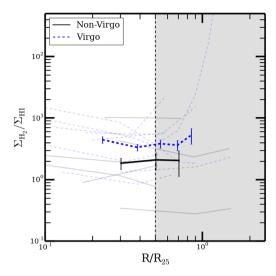
mentum and move towards the centre, into a region where it is more easily converted into molecular form. Simulations of light to moderate ram pressure stripping with cooling processes have shown that low-density gas could be preferentially removed from the outskirts while enhancing the amount of high-density gas near the centre (Tonnesen & Bryan 2009; Bekki 2014). Observations of Hickson Compact Groups have shown hints of an enhancement in the molecular gas content compared to isolated galaxies (Martinez-Badenes et al. 2012). Changes in the molecular gas distribution have been observed for the galaxies in the Abell 1367 cluster ($z = 0.022$), with some galaxies showing signs of H_2 enhancements (Scott et al. 2013, 2015).

Galaxy interactions, which are more common in the cluster environment, may also aid in this process. For example, results from the AMIGA sample of isolated galaxies suggest a possible molecular gas enhancement for interacting galaxies of approximately 0.2–0.3 dex (Lisenfeld et al. 2011).

3.3 SFR radial profiles

We present the radial profiles of the Hα-derived star formation rates in the right plot of Fig. 4. Near the central regions, there is an enhancement in the star formation rate density for the Virgo sample, similar to the trends from the H_2 profiles. The consistency between these two data sets is likely caused by the strong link between molecular gas and star formation. Previous observations have also shown that interactions can drive increases to the star formation rate (Kennicutt et al. 1987; Ellison et al. 2013), which may also contribute to the increase in the star formation rate for the Virgo sample, as several of our galaxies are in close pairs (NGC4567/NGC4568).

At large radii, there are hints of a possible truncation for Virgo galaxies, which was also seen in Koopmann et al. (2006). The behaviour of the star formation rate profiles in this region ($R/R_{25} > 1$) is less reliable, as the measurement comes from places outside where
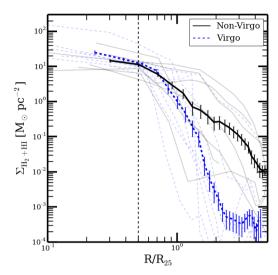
Figure 5. Left: the mean radial profiles of the H_2 to H I ratio for the galaxies in our sample, calculated using the geometric mean method and normalized by R_{25}. The statistical error bars for each profile are plotted. The individual galaxy profiles are in the background. The sample is separated into the non-Virgo (black) and Virgo (blue-dashed) populations. The dashed vertical line is at $R_{25} = 0.5$, the main target area of the NGLS survey, and results from the CO $J = 3 - 2$ maps are less reliable in the shaded region. The H_2 to H I ratio shows an enhancement for Virgo galaxies, especially near the centre. Right: the radial profiles of the total gas surface density for the galaxies in our sample, calculated using the geometric mean method and normalized by R_{25}. The statistical error bars for each profile are plotted. The individual galaxy profiles are in the background. There is a steeper radial distribution for the Virgo galaxies compared to the non-Virgo galaxies, with more gas concentrated near the centre. Ram pressure stripping is likely playing a role in removing low-density gas in the outskirts and enhancing the high-density gas near the centre.

the Hα flux is normally observed for these galaxies. The large scatter in the distribution of individual galaxy profiles is likely due to imperfect removal of other sources (such as stars) and potential differences in the neighbourhoods of these galaxies.

3.4 Environmental trends in the spatial distribution of the ISM

In Fig. 5, we present the results of the H_2/H I and H_2 + H I profiles for the smaller sample of 15 galaxies with both sets of measurements. We find that the Virgo galaxies generally have a higher H_2/H I ratio than the non-Virgo galaxies, which is also seen in a comparison of the integrated measurements from Mok et al. (2016). The non-Virgo galaxies have a relatively flat profile, at a value of around unity in the region where both H_2 and H I are detected. Due to the small number of CO $J = 3 - 2$ detected galaxies for the non-Virgo sample and the procedure used in the creation of the radial profiles, we do not probe this ratio in the central region. For the Virgo galaxies, the H_2/H I ratio rises towards the centre as expected, marking the transition to a molecular gas dominated regime. On the other hand, the slight increase in the H_2/H I ratio for the Virgo galaxies at large radii is likely not significant, as it falls in the region beyond the main NGLS survey area.

For the total gas surface density (H_2 + H I) profile, we find differences between the Virgo and non-Virgo samples. Near the centre, the non-Virgo sample has a flatter profile than the Virgo sample, due to the strong contribution from the molecular gas component. In the outskirts, the truncation in the H I discs observed for the profiles of Virgo galaxies is largely responsible for their steep total gas profiles. Steeper H_2 profiles have also been found for Virgo galaxies from the HeViCS (Pappalardo et al. 2012), especially for H I-deficient galaxies, and they fit with the idea that ram pressure stripping may be preferentially removing gas in the outskirts and enhancing the high-density gas near the centre, as discussed for the H_2 surface density profiles.
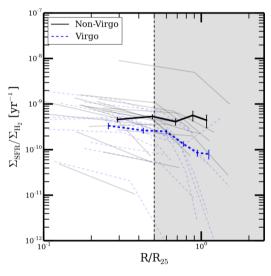

Figure 6. The SFR/H_2 surface density radial profiles for the galaxies in our sample, calculated using the geometric mean method and normalized by R_{25}. The statistical error bars for each profile are plotted. The individual galaxy profiles are in the background. The sample is separated into the non-Virgo (black) and Virgo (blue-dashed) populations. The dashed vertical line is at $R_{25} = 0.5$, the main target area of the NGLS survey, and results from the CO $J = 3 - 2$ maps are less reliable in the shaded region. Both profiles show a relatively flat trend with radius, with the Virgo galaxies offset at a lower star formation efficiency (or longer molecular gas depletion time), similar to global results presented in Mok et al. (2016).

3.5 Depressed star formation efficiency at all radii in Virgo spirals

With the Hα-derived star formation rate and the H_2 data, we can calculate the star formation efficiency (or its reciprocal, the molecular gas depletion time). The results are presented in Fig. 6. From the

SFR/H$_2$ plot, we find that Virgo galaxies generally have a lower star formation efficiency. This result has also been seen in the integrated measurements from Mok et al. (2016). The profile is relatively flat in the inner regions for both samples, with a decrease at large radii for the Virgo sample. This decline in the star formation efficiency may not be physically significant, as it sits outside of the main region of the HARP instrument in the NGLS survey and is in the regime where noise corrections to the CO $J = 3 - 2$ data become important.

The flatness in the radial profiles of the star formation efficiency has been seen in previous studies, which have found near constant molecular gas depletion times for spiral galaxies (Leroy et al. 2008; Bigiel et al. 2011; Leroy et al. 2012). The absolute values are also in line with these previous results, which have usually found gas depletion times in the $\sim$2 Gyr range. As stated previously, the reduction in the star formation efficiency at larger radii is likely due to the limitations in the survey sensitivity and mapping area.

We also find an average offset in the SFR/H$_2$ plot between the Virgo and non-Virgo profiles of $\sim$40 per cent, which was also present in the integrated measurements from Mok et al. (2016). While the Virgo galaxies generally have higher molecular gas masses than the non-Virgo galaxies, they are relatively inefficient at turning this fuel into stars. One possibility to explain this result is that there are other factors in the cluster environment, such as difference in the molecular gas properties (pressure, temperature) or larger scale dynamical stabilization (Martig et al. 2009), that may be inhibiting the process of star formation in our Virgo sample. A related effect is the possible trend of star formation efficiency with stellar masses (Saintonge et al. 2011; Schruba et al. 2011), where higher mass galaxies have lower star formation efficiencies. Our Virgo sample has a slightly higher mean stellar mass (log $M_* = 10.05 \pm 0.12$) compared to the non-Virgo sample (log $M_* = 9.87 \pm 0.07$), which may contribute to this observed difference. However, given the large scatter in these relationships and the low mean stellar mass of our sample, it is hard to quantify its effect on the star formation efficiency. A final reason may be metallicity effects (Schruba et al. 2011), which could affect the observed CO intensity and hence the SFR to CO ratio. In this paper, as in other papers in the series, we have used a constant CO to H$_2$ conversion factor and a constant line ratio between CO $J = 3 - 2$ and CO $J = 1 - 0$. Since most of our galaxies are normal spiral galaxies in a small range of stellar masses, it seems unlikely they would have metallicities of more than a factor of 2 below solar, where these effects become significant (Wilson 1995; Bolatto et al. 2008).

4 CONCLUSIONS

We present an analysis of the radial profiles of a sample of 43 H I-flux selected spiral galaxies from the JCMT NGLS with resolved JCMT H$_2$ and/or VLA H I maps. This sample includes field, group and Virgo Cluster galaxies and their gaseous discs can act as important probes for environmental effects. Using this gas-rich sample of spiral galaxies, we find significant environmental variations in the spatial distribution of the ISM, including the H I and H$_2$ radial profiles, as well as in their star formation properties.

(i) We confirm that the H I discs are truncated in the Virgo sample, compared to the non-Virgo sample. This result is well known from previous studies of the atomic gas distribution inside clusters (Cayatte et al. 1994), but we also observe this same effect for these relatively gas-rich galaxies. Comparing between the smaller group and field samples, we find that there is a decrease in the H I

disc size for group galaxies compared to field galaxies, which may be related to the trends in H I properties with group masses (Jaffé et al. 2016) and suggests that the environment affects the H I gas even in moderate-density regions.

(ii) We find that the H$_2$ distribution is enhanced for Virgo galaxies, especially near the centre, which results in a significantly higher H$_2$ to H I ratio for Virgo galaxies. This matches the results found using integrated measurements of these galaxies in Mok et al. (2016). The steeper radial profile for the total gas content (H I + H$_2$), even for these gas-rich objects, suggests that the environment may play a role in determining the spatial distribution of the ISM inside these galaxies. The most likely scenario is moderate ram pressure stripping that preferentially removes low-density gas in the outskirts of these spiral galaxies and aids in the creation of higher density gas near the centre (Tonnesen & Bryan 2009). Another possibility is interactions in the Virgo sample, as enhancements in molecular gas have also been seen in interacting isolated galaxies (Lisenfeld et al. 2011) and in compact group galaxies (Martinez-Badenes et al. 2012).

(iii) The Hα star formation rate data for our galaxies show similar trends to the H$_2$ distribution. There is an enhancement in the star formation rate surface density for Virgo galaxies near the centre, which is likely related to the increase in the molecular gas surface density. Interactions in the Virgo sample, as discussed for the H$_2$ profiles, may also enhance star formation (Kennicutt et al. 1987; Ellison et al. 2013). We also find hints of an Hα truncation at large radii for Virgo galaxies, which has been found in other surveys of cluster spirals (Koopmann et al. 2006).

(iv) We find that the star formation efficiency (SFR/H$_2$) is relatively constant with radius for the Virgo and non-Virgo samples. This is consistent with the near-constant molecular gas depletion times found in other surveys for normal spiral galaxies (Bigiel et al. 2011; Leroy et al. 2012). However, the star formation efficiency for the Virgo galaxies is on average $\sim$40 per cent lower than that of non-Virgo galaxies. This variation may be the result of differences in the star formation process for Virgo galaxies or variations in the molecular gas properties (pressure, temperature, metallicity).

usage of the HyperLeda data base (http://leda.univ-lyon1.fr). This research has made use of the GOLDMine Database. This research has made use of data from the HRS project. HRS is a Herschel Key Programme utilizing Guaranteed Time from the SPIRE instrument team, ESAC scientists and a mission scientist. The HRS data was accessed through the Herschel Database in Marseille (HeDaM – http://hedam.lam.fr) operated by CeSAM and hosted by the Laboratoire d'Astrophysique de Marseille.

The Digitized Sky Surveys were produced at the Space Telescope Science Institute under US Government grant NAG W-2166. The images of these surveys are based on photographic data obtained using the Oschin Schmidt Telescope on Palomar Mountain and the UK Schmidt Telescope. The plates were processed into the present compressed digital form with the permission of these institutions. The National Geographic Society – Palomar Observatory Sky Atlas (POSS-I) was made by the California Institute of Technology with grants from the National Geographic Society. The Second Palomar Observatory Sky Survey (POSS-II) was made by the California Institute of Technology with funds from the National Science Foundation, the National Geographic Society, the Sloan Foundation, the Samuel Oschin Foundation and the Eastman Kodak Corporation. The Oschin Schmidt Telescope is operated by the California Institute of Technology and Palomar Observatory. The UK Schmidt Telescope was operated by the Royal Observatory Edinburgh, with funding from the UK Science and Engineering Research Council (later the UK Particle Physics and Astronomy Research Council), until 1988 June, and thereafter by the Anglo–Australian Observatory. The blue plates of the southern Sky Atlas and its Equatorial Extension (together known as the SERC-J), as well as the Equatorial Red (ER), and the Second Epoch (red) Survey (SES) were all taken with the UK Schmidt.

REFERENCES

Bekki K., 2014, MNRAS, 438, 444
Bigiel F. et al., 2011, ApJ, 730, L13
Blanton M. R., Moustakas J., 2009, ARA&A, 47, 159
Bolatto A. D., Leroy A. K., Rosolowsky E., Walter F., Blitz L., 2008, ApJ, 686, 948
Boselli A., Cortese L., Boquien M., Boissier S., Catinella B., Gavazzi G., Lagos C., Saintonge A., 2014, A&A, 564, A67
Boselli A., Fossati M., Gavazzi G., Ciesla L., Buat V., Boissier S., Hughes T. M., 2015, A&A, 579, A102
Cayatte V., van Gorkom J. H., Balkowski C., Kotanyi C., 1990, AJ, 100, 604
Cayatte V., Kotanyi C., Balkowski C., van Gorkom J. H., 1994, AJ, 107, 1003
Chung A., van Gorkom J. H., Kenney J. D. P., Crowl H., Vollmer B., 2009, AJ, 138, 1741
Dressler A., 1980, ApJ, 236, 351
Ellison S. L., Mendel J. T., Patton D. R., Scudder J. M., 2013, MNRAS, 435, 3627
Gavazzi G., Fumagalli M., Galardo V., Grossetti F., Boselli A., Giovanelli R., Haynes M. P., Fabello S., 2012, A&A, 545, A16
Gunn J. E., Gott J. R., III, 1972, ApJ, 176, 1
Haynes M. P., Giovanelli R., 1986, ApJ, 306, 466
Huang M.-L., Kauffmann G., 2014, MNRAS, 443, 1329
Jaffé Y. L. et al., 2016, MNRAS, 461, 1202
Kenney J. D. P., Young J. S., 1989, ApJ, 344, 171
Kennicutt R. C. Jr., Roettiger K. A., Keel W. C., van der Hulst J. M., Hummel E., 1987, AJ, 93, 1011
Kennicutt R. C. Jr., et al., 2009, ApJ, 703, 1672
Koopmann R. A., Haynes M. P., Catinella B., 2006, AJ, 131, 716
Kroupa P., Weidner C., 2003, ApJ, 598, 1076
Larson R. B., Tinsley B. M., Caldwell C. N., 1980, ApJ, 237, 692
Leroy A. K., Walter F., Brinks E., Bigiel F., de Blok W. J. G., Madore B., Thornley M. D., 2008, AJ, 136, 2782
Leroy A. K. et al., 2012, AJ, 144, 3
Lisenfeld U. et al., 2011, A&A, 534, A102
Luo Y., Kang X., Kauffmann G., Fu J., 2016, MNRAS, 458, 366
McGee S. L., Balogh M. L., Bower R. G., Font A. S., McCarthy I. G., 2009, MNRAS, 400, 937
Makarov D., Prugniel P., Terekhova N., Courtois H., Vauglin I., 2014, A&A, 570, A13
Martig M., Bournaud F., Teyssier R., Dekel A., 2009, ApJ, 707, 250
Martinez-Badenes V., Lisenfeld U., Espada D., Verdes-Montenegro L., García-Burillo S., Leon S., Sulentic J., Yun M. S., 2012, A&A, 540, A96
Mok A. et al., 2016, MNRAS, 456, 4384
Moore B., Katz N., Lake G., Dressler A., Oemler A., 1996, Nature, 379, 613
Norris N., 1940, Ann. Math. Stat., 11, 445
Pappalardo C. et al., 2012, A&A, 545, A75
Paturel G., Petit C., Prugniel P., Theureau G., Rousseau J., Brouty M., Dubois P., Cambrésy L., 2003, A&A, 412, 45
Peng Y.-j. et al., 2010, ApJ, 721, 193
Peng Y.-j., Lilly S. J., Renzini A., Carollo M., 2012, ApJ, 757, 4
Saintonge A. et al., 2011, MNRAS, 415, 61
Sánchez-Gallego J. R., Knapen J. H., Wilson C. D., Barmby P., Azimlu M., Courteau S., 2012, MNRAS, 422, 3208
Schruba A. et al., 2011, AJ, 142, 37
Scott T. C., Usero A., Brinks E., Boselli A., Cortese L., Bravo-Alfaro H., 2013, MNRAS, 429, 221
Scott T. C., Usero A., Brinks E., Bravo-Alfaro H., Cortese L., Boselli A., Argudo-Fernández M., 2015, MNRAS, 453, 328
Strong A. W. et al., 1988, A&A, 207, 1
Tonnesen S., Bryan G. L., 2009, ApJ, 694, 789
Walter F., Brinks E., de Blok W. J. G., Bigiel F., Kennicutt R. C. Jr., Thornley M. D., Leroy A., 2008, AJ, 136, 2563
Wilson C. D., 1995, ApJ, 448, L97
Wilson C. D. et al., 2012, MNRAS, 424, 3050

This paper has been typeset from a TEX/LATEX file prepared by the author.